

Supplementary Information 4:

Scaling structural carbon

Tim Rademacher

13/11/2020

*This pdf was generated from an Rmarkdown file, which includes all R code necessary to reproduce the estimations. The Rmarkdown file is available on github:
<https://github.com/TTRademacher/Exp2017Analysis>.*

Structural carbon estimation for stem sections

We estimate structural carbon gain for each stem section and period from the cell-wall area estimated to have formed in that period. The cell-wall area of one thinsection sampled at the end of the growing season (3rd November 2017) was therefore divided into sections grown between sampling dates (e.g., prior, during and after treatment) by association with the fraction of the ring formed at each sampling date. For each sampling date two microcores were collected with trephor tool (Rossi et al., 2006). Microcores in August, October and November were punched in close proximity to the July sample. However, the samples were offset by, at least, 5cm horizontally on the same vertical axis to avoid sampling a wound reaction of the injury inflicted by previous cores. As growth varies locally around the circumference of the stem, sampling relatively close was a first step to minimised local differences in growth between sampling dates. One of those microcores was embedded in paraffin (Tissue Processor 1020 Leica, Switzerland) and 7 μm -thick crosssectional cuts were obtained using a rotary microtome (Leica RM2245, Switzerland). The cuts were stained with astra blue and safranin red, and scanned on a sliding scanner (resolution of roughly 1.5 μm). Where the resulting image of the first microcore did not fully include the necessary rings or had other quality issues, we cut and processed the second microcore. Between the two microcores, we were able to obtain high-quality image data for 315 out of 320 samples (i.e., 4 sampling dates times 40 trees times on average two sampling heights). Only for one tree (tree id: 06; treatment: control) both thinsections collected in October did not contain a full set of rings necessary for the analysis. For each image, we identified and divided the ring formed in 2017 into 20 μm -wide discrete tangential bands and derived the average anatomical structure for cells in each band using ROXAS (Arx and Carrer, 2014). In particular, we measured average cell-wall area, cell-wall thickness, as well as tangential and radial lumen diameter. The ring width of the fully formed 2017 ring ranged between 0.42 and 3.23 mm with a mean of 1.64 mm. Even the smallest ring was divided into 21 discrete bands of a width of 20- μm with associated anatomical data.

Estimating period of formation of tangential bands

Ring widths were measured for all sampling dates using the self-developed Wood Image Analysis and Database platform (<http://wiad.science>). The ring widths were standardised to account for local variations in growth in thinsections. Standardised ring widths from the different sampling dates were then used to associate proportions of the final ring from the November microcore (i.e., which 20 μm -wide band to include), to specific growth periods. For this purpose we identified and measured ring widths in thinsections taken prior (e.g., 3rd of July 2017) and during the treatment (e.g., 10th of August 2017, and 9th of October 2017), as well as at the end of the growing season (3rd of November). For standardisation, we used the width of an older ring from the same thinsection to correct for local variation in growth between microcores.

$$f_{m,17} = \frac{rw_{m,17} \times rw_{end,15}}{rw_{m,15}} \times \frac{1}{rw_{end,17}}$$

, where $f_{m,17}$ is the fraction of the ring width formed in month m (e.g., July, August, or October), $rw_{m,15}$ and $rw_{m,17}$ are respectively the 2015 and 2017 ring width in the thinsection collected in month m , and $rw_{end,15}$ and $rw_{end,17}$ are respectively the 2015 and 2017 ring widths in the thinsection from the November sample. This assumes that the ring was fully formed on the 3rd of November, which is about two weeks after the typical end of cell wall thickening for white pine at Harvard Forest. Then, $f_{m,17}$ theoretically varies between 0 and 1 with 0 meaning none of the ring was formed at the sampling date and 1 meaning that the entire ring was already formed.

The number of measurements for growth rings drops off strongly after the 2015 growth ring (table 1), because the older rings are further away from the bark, hence they are less likely within the 15mm reach of the trephor tool (Rossi et al., 2006) used to collect the microcores. Among the recent years with high replication, 2015 was preferred over 2016, because of an abnormally dry growing season in 2016 (total annual precipitation of 936 mm, which is 160 below the long-term average of 1096 mm). In fact, about three quarters of trees included in this study showed an intra-annual density fluctuation in 2016 due to the dry growing season and the remaining quarter of trees had a relatively narrower ring. 2016 was 0.90 °C warmer with 234 mm less precipitation compared to the 30-year average. Consequently, standardisation by the 2016 ring would introduce a systematic bias based on the bi-modal ring width distribution in 2016. In contrast, 2015 did not include any outstanding climatological events or resulting systematic bias in growth. Indeed, the 2015 growing season climate was similar to the 2017 growing season climate with a mean annual temperature of 8.1 °C and a total annual precipitation of 1024 mm. Both 2017 and 2015 were close to the long-term averages mentioned above.

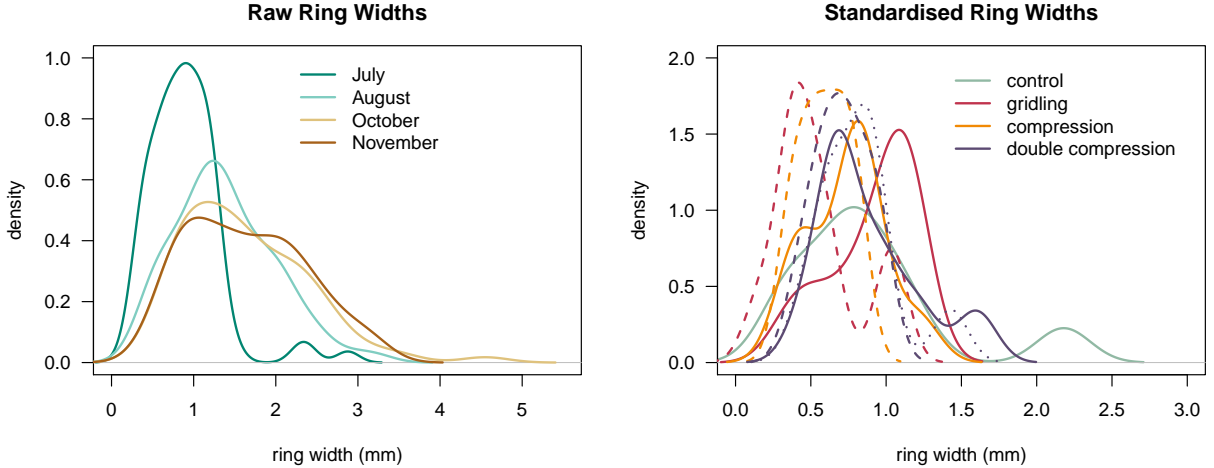


Table 1: Number of measured growth ring widths for all trees out of a potential 320 thinsection images.

	2017	2016	2015	2014	2013	2012	2011	2010	2009	2008
Number of Samples	320.00	319.00	315.00	282.00	209.00	115.00	49.0	31.0	9.0	0
Percentage	100.00	99.70	98.40	88.10	65.30	35.90	15.3	9.7	2.8	0
Mean Ring Width (mm)	1.71	1.83	2.35	2.07	1.55	1.85	NaN	NaN	NaN	NaN

On average, 55%, 83.7%, and 101.6% of the ring width had respectively grown in July, August and October. Thus, a bit more than half of the ring widths was already formed before the start of the treatment and ring width growth had *de facto* finished by October. However, there were substantial differences between

treatments and sampling heights in the timeline of xylogenesis.

Using the fractional ring widths as boundaries, each 20- μm band was associated with one of the four periods: (1) beginning of growing season to start of experiment (3rd of July 2017), (2) first month of the experiment (4th of July to 9th of August 2017), (3) second month of the experiment (10th of August to 8th of October 2017), (4) end of double compression to end of growing season (9th of October to 3rd of November 2017). These period are illustrated in Fig. 1 (main manuscript).

We acknowledge that radial volume growth is insufficiently captured by merely using tree ring fractions at four dates throughout the growing season to determine detailed phenological progressions or high resolution xylogenetic dynamics (e.g., weekly). For better temporal attribution, especially towards the asymptotic tails of the growing season, more measurement dates would be needed. Therefore, we focus on large patterns in our analysis, which are robust, due to the sequential nature of radial growth, and do not depend on the precise estimation of the date of formation of any one tangential band. Future studies incorporating more frequent sampling and the use General Additive Models to fit intra-annual growth trends, would be better suited to attribute temporal variations in growth.

Scaling measured cell wall area to stem section

After we associated each tangential band with a growth period, each band is scaled to the circumference of the stem section by multiplication of the mean zonal cell-wall area by the number of times the average zonal tangential cell width ($w_{t,s}$) fits into the entire circumference of each stem section. To account for the bark (assuming a bark thickness of 0.8cm) we reduced the circumference, as measured at the beginning of the experiment ($CBH_{outer,s}$) according to the following equation:

$$CBH_s = CBH_{outer,s} - 0.8cm \times 2\pi$$

The zonal cell wall area for each band is then summed across fractions of the ring were previously associated with the same period of formation. As a result we obtain an estimate of the total cell wall area formed during each period.

To further scale the total circumferential cell-wall area to a cell-wall volume per stem section, we assume that the measured cell-wall area ($CWA_{s,p}$) is representative of the longitudinal wood profile for the stem section, hence we can simply multiply it with the height of the stem section ($h = 10cm$).

$$V_{CW,s,p} = \frac{CBH_s}{w_{t,s}} \times h_s \times C\bar{W}A$$

Implicitly, this approach assumes that wood is circumferentially and longitudinally homogenous and the measured tracheids are representative of the woody tissue. thus, the approach does not account for other types of tissue than tracheids, such as rays and resin ducts. Tracheids make up 93% of the volume of wood in white pines with resin ducts and rays accounting for 1% and 6%, respectively (Brown et al., 1949). However, since there was no clear treatment effect on the occurrence of resin ducts or rays cells, this assumption should not introduce a bias in carbon sequestration in structure between treatments. As ray cells and resin ducts have a slightly lower carbon density, this approach does, however, over estimate carbon density marginally.

Finally, the cell-wall volume for each ring portion of the stem section ($V_{CW,s,p}$) is multiplied by a fixed cell-wall density (ρ_{CW}) of 1.489 $kg\ m^{-3}$ (measured for Scots pine by Plötze and Niemz (2011)) and a carbon content of 49.74% typical of white pine (Lamblom and Savidge, 2003) to estimate the total structural carbon gain per stem section and period ($M_{p,s}$ in g).

$$M_{s,p} = V_{CW,s,p} \times \rho_{CW} \times 49.74\%$$

Alternative estimate using wood density

To better understand uncertainties associated with our assumptions we also used an alternative estimate based on wood density. For this alternative estimation, the carbon is simply estimated as a product of the volume of wood and an average wood density. To obtain wood density values, X-ray densitometry was performed on 18 increment cores from the ten control trees.

References

- Arx, G. von, Carrer, M., 2014. ROXAS – A new tool to build centuries-long tracheid-lumen chronologies in conifers. *Dendrochronologia* 32, 290–293.
- Brown, H., Panshin, A., Forsaith, C., 1949. Textbook of Wood Technology, First Edition. ed, American Forestry Series. McGraw-Hill Book Company, Inc.
- Lamloom, S., Savidge, R., 2003. A reassessment of carbon content in wood: Variation within and between 41 North American species. *Biomass and Bioenergy* 25, 381–388.
- Plötze, M., Niemz, P., 2011. Porosity and pore size distribution of different wood types as determined by mercury intrusion porosimetry. *European Journal of Wood and Wood Products* 69, 649–657.
- Rossi, S., Anfodillo, T., Menardi, R., 2006. Trephor: A New Tool for Sampling Microcores from tree stems. *IAWA Journal* 89–97.